Science
AAAS

Supramolecular Linear Heterojunction Composed of Graphite-Like Semiconducting Nanotubular Segments

Wei Zhang, *et al.*

Science **334**, 340 (2011);
DOI: 10.1126/science.1210369

This copy is for your personal, non-commercial use only.

If you wish to distribute this article to others, you can order high-quality copies for your colleagues, clients, or customers by clicking here.

Permission to republish or repurpose articles or portions of articles can be obtained by following the guidelines here.

The following resources related to this article are available online at www.sciencemag.org (this infomation is current as of November 14, 2011):

Updated information and services, including high-resolution figures, can be found in the online version of this article at:
http://www.sciencemag.org/content/334/6054/340.full.html

Supporting Online Material can be found at:
http://www.sciencemag.org/content/suppl/2011/10/19/334.6054.340.DC1.html

A list of selected additional articles on the Science Web sites **related to this article** can be found at:
http://www.sciencemag.org/content/334/6054/340.full.html#related

This article **cites 30 articles**, 6 of which can be accessed free:
http://www.sciencemag.org/content/334/6054/340.full.html#ref-list-1

This article appears in the following **subject collections:**
Materials Science
http://www.sciencemag.org/cgi/collection/mat_sci

Downloaded from www.sciencemag.org on November 14, 2011

Science (print ISSN 0036-8075; online ISSN 1095-9203) is published weekly, except the last week in December, by the American Association for the Advancement of Science, 1200 New York Avenue NW, Washington, DC 20005. Copyright 2011 by the American Association for the Advancement of Science; all rights reserved. The title *Science* is a registered trademark of AAAS.

21. B. P. Bonev *et al.*, *Astrophys. J.* **661**, L97 (2007).
22. H.-H. Limbach *et al.*, *ChemPhysChem* **7**, 551 (2006).
23. S. Andersson, E. F. van Dishoeck, *Astron. Astrophys.* **491**, 907 (2008).
24. Y. Shinnaka *et al.*, *Astrophys. J.* **729**, 81 (2011).
25. S. J. Weidenschilling, *Mon. Not. R. Astron. Soc.* **180**, 57 (1977).
26. S. A. Sandford *et al.*, *Science* **314**, 1720 (2006).
27. D. H. Wooden, *Space Sci. Rev.* **138**, 75 (2008).

Acknowledgments: Herschel is a European Space Agency space observatory with science instruments provided by European-led principal investigator consortia and with important participation from NASA. This work was partially supported by Nederlandse Organisatie voor Wetenschappelijk Onderzoek grant 639.042.404, NSF grant 0707777, and, as part of the NASA Herschel HIFI guaranteed time program, NASA. The data presented here are archived at the Herschel Science Archive, http://archives.esac.esa.int/hda/ui, under OBSID 1342198337 and 1342201585.

Supporting Online Material
www.sciencemag.org/cgi/content/full/334/6054/338/DC1
Materials and Methods
Table S1
References (*28*–*39*)

25 May 2011; accepted 20 September 2011
10.1126/science.1208931

Supramolecular Linear Heterojunction Composed of Graphite-Like Semiconducting Nanotubular Segments

Wei Zhang,[1,2] Wusong Jin,[3] Takanori Fukushima,[1,4]* Akinori Saeki,[5] Shu Seki,[5] Takuzo Aida[1,2]*

One-dimensionally connected organic nanostructures with dissimilar semiconducting properties are expected to provide a reliable platform in understanding the behaviors of photocarriers, which are important for the development of efficient photon-to-electrical energy conversion systems. Although bottom-up supramolecular approaches are considered promising for the realization of such nanoscale heterojunctions, the dynamic nature of molecular assembly is problematic. We report a semiconducting nanoscale organic heterojunction, demonstrated by stepwise nanotubular coassembly of two strategically designed molecular graphenes. The dissimilar nanotubular segments, thus connected noncovalently, were electronically communicable with one another over the heterojunction interface and displayed characteristic excitation energy transfer and charge transport properties not present in a mixture of the corresponding homotropically assembled nanotubes.

Heterojunctions, occurring between two dissimilar semiconducting materials, are expected to provide peculiar electronic properties that are hard to realize by homojunctions. Heterojunctions of varying dimensions are readily fabricated from inorganic semiconductors and lead to many applications, including solid-state lasers, diodes, solar cells, and transistors (*1*–*6*). Organic heterojunctions are of importance in the development of organic thin-film solar cells (*7*, *8*). However, most that have been studied are so-called bulk heterojunctions, which are formed only coincidentally from donor/acceptor mixtures upon phase separation (*9*–*12*). Although bottom-up supramolecular approaches (*13*, *14*) are a potent tool for the formation of organic heterojunctions, such studies have just started with molecularly engineered donor/acceptor couples (*15*–*19*). From a fundamental viewpoint, one challenge would be to tailor a linear organic heterojunction at the nanoscale by joining together dissimilar semiconducting one-dimensional molecular objects, because one has to overcome the essential problem arising from the dynamic nature of molecular assembly (*13*, *14*, *20*–*24*).

We reported that a Gemini-shaped hexa-*peri*-hexabenzocoronene (HBC) derivative, bearing two triethylene glycol-appended phenyl groups on one side of the HBC core and dodecyl side chains on the other, self-assembles into a semiconducting nanotube with inner and outer diameters of 14 and 20 nm, respectively (*25*, *26*). A recent structural analysis using a synchrotron x-ray diffraction technique revealed that the nanotube is composed of a graphite-like bilayer wall consisting of helically twisted columnar arrays of π-stacked HBC units (*26*). For the realization of a nanotubular heterojunction using this self-assembling motif, essential requisites are (i) the formation of a morphologically stabilized seed nanotube and (ii) the design of a second graphene monomer capable of tubularly assembling from the extremely thin facets of the seed nanotube termini. Further issues include how to cope with a high dispersibility of the seed nanotube and a solubility of the second monomer under assembling conditions.

A keen examination, taking into account all the above requisites, led us to HBC derivatives **1** and **2** (*27*) as the monomers for the seed and second nanotubular segment, respectively (Fig. 1). HBC **1** carries two bipyridine (bpy) units, in order for the resulting seed nanotube (Fig. 1A) to be morphologically stabilized by wrapping with a metal-coordination network (Fig. 1 B) (*28*). The charged surface of the resultant seed also merits its homogeneous dispersion by an electrostatic repulsion (*29*). On the other hand, HBC **2** bears four electron-withdrawing fluorine substituents, so it can adhere electronically to the seed termini and self-assemble selectively from their nanotubular facets. When these HBC molecules coassemble stepwise (Fig. 1C), the resultant connecting segments are electronically dissimilar to one another (Fig. 1D).

As a typical example of the preparation of the seed nanotube (**NT$_{1\bullet Cu}$**, Fig. 1B), a 5-ml glass vial containing a tetrahydrofuran (THF) solution (2.0 ml) of HBC **1** (0.5 mg, 1.5×10^{-4} M) was placed in a 50-ml glass vial containing 10 ml of methanol (MeOH) and allowed to stand at 25°C, whereupon a yellow suspension gradually formed. Absorption spectroscopy of the suspension after a 24-hour incubation (fig. S1, A and B, broken curve) showed red-shifted absorption bands at 426 and 459 nm characteristic of *J*-aggregated HBCs (*25*, *26*). Scanning electron microscopy (SEM, fig. S2A) and transmission electron microscopy (TEM, fig. S2B) of an air-dried sample of the suspension allowed for visualizing nanotubes (**NT$_1$**) with a uniform diameter of 20 nm, although they were heavily bundled (Fig. 1A) just like other HBC nanotubes (*25*, *26*). We investigated the metal-coordination capability of **NT$_1$** by using Cu^{2+}, because bpy is known to bind to Cu^{2+}, affording a bpy$_2$•Cu^{2+} complex. As soon as a MeOH solution (1.0 ml) of copper(II) trifluoromethanesulfonate [$Cu(OTf)_2$, 0.5 mg, 1.5×10^{-6} mol; 5.0 equivalents to HBC **1**] was added, the suspension containing bundled **NT$_1$** became clear, suggesting that Cu^{2+} ions are bound to the surface bpy groups (Fig. 1, A to B) and make the nanotubes (**NT$_{1\bullet Cu}$**) electrostatically repulsive from one another (*29*). When an air-dried sample of **NT$_{1\bullet Cu}$**, isolated by filtration and washed with MeOH to remove free $Cu(OTf)_2$, was subjected to SEM, highly dispersed nanotubes were observed (fig. S3A). Complete coordination of Cu^{2+} with bpy-appended HBC **1** was confirmed by matrix-assisted laser desorption ionization time-of-flight (MALDI-TOF) mass spectrometry of isolated **NT$_{1\bullet Cu}$** (fig. S4); no peaks attributable to metal-free **1** were detected, but those assignable to **1•Cu**, dissociated from **NT$_{1\bullet Cu}$**, were. The metal coordination of **NT$_1$** did not give rise to any shift of the *J*-aggregate absorption bands (426 and 459 nm; fig. S1B, solid curve). Hence, the π-stacking geometry of the HBC units is intact

[1]Functional Soft Matter Research Group, RIKEN Advanced Science Institute, 2-1 Hirosawa, Wako, Saitama 351-0198, Japan. [2]Department of Chemistry and Biotechnology, School of Engineering, The University of Tokyo, 7-3-1 Hongo, Bunkyo-ku, Tokyo 113-8656, Japan. [3]College of Chemistry, Chemical Engineering and Biotechnology, Donghua University, 2999 North Renmin Road, Songjiang, Shanghai 201620, People's Republic of China. [4]Chemical Resources Laboratory, Tokyo Institute of Technology, 4259 Nagatsuta, Midori-ku, Yokohama 226-8503, Japan. [5]Graduate School of Engineering, Osaka University, 2-1 Yamadaoka, Suita, Osaka 565-0871, Japan.

*To whom correspondence should be addressed. E-mail: fukushima@riken.jp (T.F.); aida@macro.t.u-tokyo.ac.jp (T.A.)

Downloaded from www.sciencemag.org on November 14, 2011

even with the formation of a metal-coordination network on the nanotube surface.

We investigated whether HBC **2** alone has the ability to form a nanotubular assembly. On the basis of a computational study using density functional theory (DFT), the core of HBC **2** with four fluorine substituents most likely adopts a slightly twisted, concave structure (fig. S5). Probably because of this skeletal distortion, HBC **2** was unable to assemble into nanotubes under a variety of conditions used previously (*16*, *18*, *25*, *26*, *28*, *29*). However, we eventually found that, in acetone, **2** self-assembles into tubules. This observation was unexpected because none of other reported HBC derivatives assemble to form nanotubes in acetone. For the nanotubular assembly of **2**, an acetone suspension of this HBC (1.5×10^{-4} M) was heated to 50°C, and the resultant clear solution was allowed to cool to 25°C. The solution gradually became turbid and displayed a red-shifted absorption spectrum characteristic of *J*-aggregated HBCs (fig. S1, C and D). SEM of an air-dried sample of the suspension, obtained after a 12-hour incubation, showed the presence of heavily bundled cylindrical nanostructures (fig. S6A). TEM revealed that the cylinders are actually nanotubes ($\mathbf{NT_2}$) with a uniform diameter of 20 nm (fig. S6B).

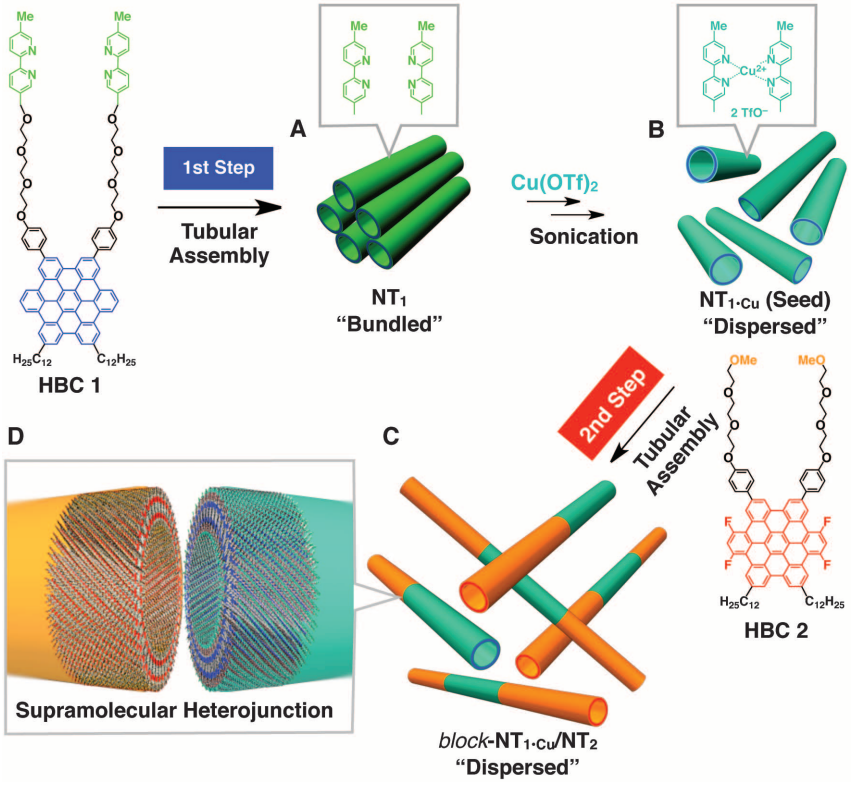

Fig. 1. Molecular structures of HBCs **1** and **2** and schematic illustrations of the preparation of (**A**) $\mathbf{NT_1}$ (bundled) by MeOH vapor diffusion into a THF solution of HBC **1**, (**B**) seed $\mathbf{NT_{1•Cu}}$ (dispersed) by post-functionalization of $\mathbf{NT_1}$ with $Cu(OTf)_2$ in MeOH, and (**C**) *block*-$\mathbf{NT_{1•Cu}/NT_2}$ (dispersed) by cooling a hot acetone solution of HBC **2** in the presence of $\mathbf{NT_{1•Cu}}$ as the seed. (**D**) Schematic illustration of an idealized cross section of *block*-$\mathbf{NT_{1•Cu}/NT_2}$ at the heterojunction interface.

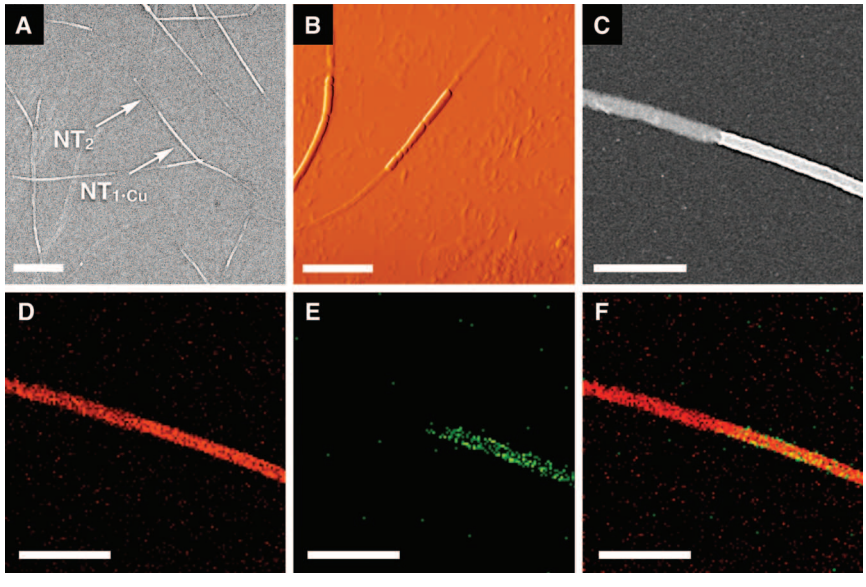

Fig. 2. Microscopic imaging of *block*-$\mathbf{NT_{1•Cu}/NT_2}$ ([**2**]/[**1**] = 1.0). The sample was prepared by drop-casting its acetone dispersion and air dried. (**A**) SEM (scale bar, 500 nm), (**B**) tapping-mode AFM (scale bar, 200 nm), and (**C**) scanning TEM (scale bar, 50 nm) micrographs. TEM-EDX mapping of (**D**) carbon (scale bar, 50 nm), (**E**) copper (scale bar, 50 nm), and (**F**) carbon and copper elements (scale bar, 50 nm).

The $\mathbf{NT_{1•Cu}}$ dispersed individually in acetone, where the nanotubular assembly of HBC **2** can occur. As a typical example of the successful heterojunction (Fig. 1C), the acetone dispersion of $\mathbf{NT_{1•Cu}}$, used as the seed (Fig. 1B), was presonicated for 5 to 10 min so that the nanotubes were cut into short pieces for enhancing the probability of linear heterojunction (fig. S3C). The resultant dispersion of $\mathbf{NT_{1•Cu}}$ (1.5×10^{-4} M, 1.0 ml) was mixed at 50°C with an acetone solution of HBC **2** (1.5×10^{-4} M, 1.0 ml). When the mixture was allowed to cool and stand at 25°C, the assembly of HBC **2** took place. The self-assembly of **2** without $\mathbf{NT_{1•Cu}}$ gave rise to a suspension of bundled $\mathbf{NT_2}$. However, the co-assembling mixture in the presence of $\mathbf{NT_{1•Cu}}$ remained clear even after 12 hours. When an air-dried sample of this clear dispersion was studied by SEM, micrometer-long nanotubular objects with bright and dark segments were observed (Fig. 2A and fig. S7). Most of the nanotubes appeared to consist of two block segments, but some were composed of three block segments. Likewise, scanning TEM allowed for visualizing the presence of segments with different contrasts in single nanotubes (Fig. 2C). By means of element mapping using TEM energy-dispersive x-ray spectroscopy (TEM-EDX), we confirmed that copper is localized in the bright segments (Fig. 2, E and F), whereas carbon populates over the entire nanotube (Fig. 2, D and F). These observations demonstrate the occurrence of a linear heterojunction to give *block*-$\mathbf{NT_{1•Cu}/NT_2}$ (Fig. 1C). Considering the electronic characters of the two HBC molecules, the heterotropic π-stacking interaction seems stronger than the homotropic one. This drives the preferential assembly of HBC **2** on the nanotubular facets of seed $\mathbf{NT_{1•Cu}}$. Because multiblock heterojunction nanotubes such as $\mathbf{NT_{1•Cu}}$–$\mathbf{NT_2}$–$\mathbf{NT_{1•Cu}}$–$\mathbf{NT_2}$ and $\mathbf{NT_{1•Cu}}$–$\mathbf{NT_2}$–$\mathbf{NT_{1•Cu}}$ were not detected, postconnection of $\mathbf{NT_2}$ with $\mathbf{NT_{1•Cu}}$ is unlikely. In tapping-mode atomic force microscopy (AFM) on a silicon wafer, these two block segments exhibited different height profiles, 16 to 18 nm and 8 to 10 nm (Fig. 2B),

Downloaded from www.sciencemag.org on November 14, 2011

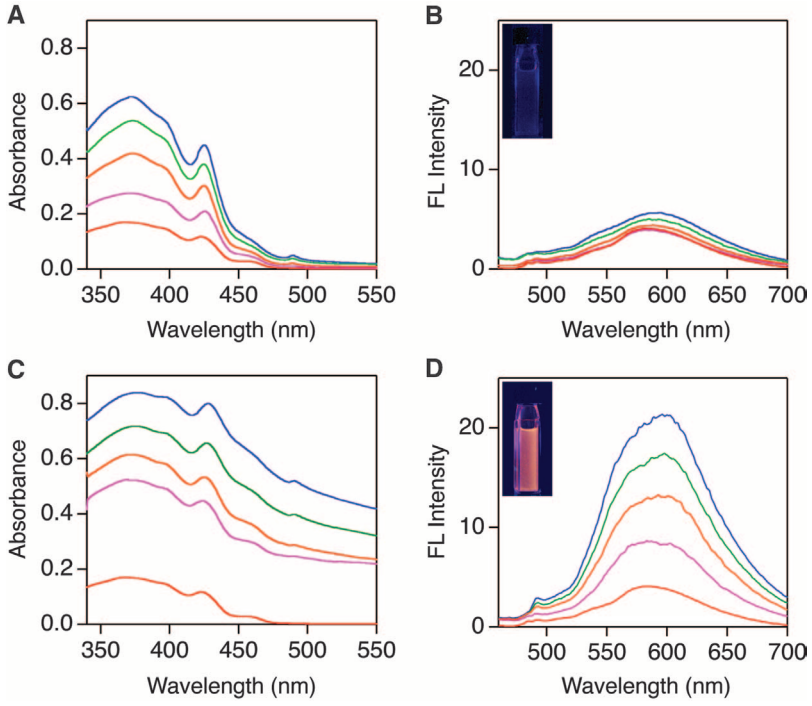

Fig. 3. (**A**) Absorption and (**B**) fluorescence spectra in acetone at 25°C of *block*-$\mathbf{NT_{1\cdot Cu}/NT_2}$ prepared by using different molar ratios of **2** to **1** for their stepwise coassembly {[**1**] = 1.5×10^{-4} M; [**2**] = 0 (red), 0.75×10^{-4} M (pink), 1.5×10^{-4} M (orange), 2.3×10^{-4} M (green), and 3.0×10^{-4} M (blue)}. (B inset) A photograph of an acetone dispersion of *block*-$\mathbf{NT_{1\cdot Cu}/NT_2}$ ([**2**]/[**1**] = 1.0) upon 365-nm excitation. (**C**) Absorption and (**D**) fluorescence spectra in acetone at 25°C of mixtures of $\mathbf{NT_{1\cdot Cu}}$ and $\mathbf{NT_2}$ at different molar ratios of **2** to **1** {[**1**] = 1.5×10^{-4} M; [**2**] = 0 (red), 0.75×10^{-4} M (pink), 1.5×10^{-4} M (orange), 2.3×10^{-4} M (green), and 3.0×10^{-4} M (blue)}. (D inset) A photograph of an acetone suspension of a mixture of $\mathbf{NT_{1\cdot Cu}}$ and $\mathbf{NT_2}$ ([**2**]/[**1**] = 1.0) upon 365-nm excitation. The baseline uprise in (C) upon increment of [**2**] is due to light scattering by bundled $\mathbf{NT_2}$.

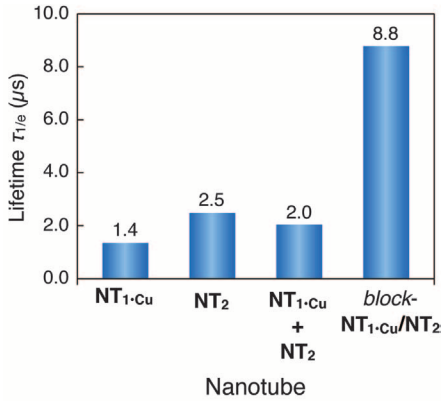

Fig. 4. Lifetimes ($\tau_{1/e}$) of charge carriers generated by laser excitation of $\mathbf{NT_{1\cdot Cu}}$, $\mathbf{NT_2}$, a mixture of $\mathbf{NT_{1\cdot Cu}}$ and $\mathbf{NT_2}$ ([**2**]/[**1**] = 1.0), and *block*-$\mathbf{NT_{1\cdot Cu}/NT_2}$ ([**2**]/[**1**] = 1.0) in the solid state. $\tau_{1/e}$ is defined by the time when the FP-TRMC transient decays down to 1/*e* of its maximum value (fig. S10).

that were the same as those observed for separately prepared homotropic $\mathbf{NT_{1\cdot Cu}}$ and $\mathbf{NT_2}$ (fig. S8). The exceptionally small height profile of $\mathbf{NT_2}$ indicates a low structural robustness of its graphite-like wall because of the nonplanar HBC core of **2** (fig. S5).

As shown in fig. S9, $\mathbf{NT_1}$ (black solid curve) and $\mathbf{NT_2}$ (black broken curve), when photoexcited at 365 nm, fluoresced most intensely at 585 and 594 nm, respectively (*16*, *18*, *29*). In sharp contrast, $\mathbf{NT_{1\cdot Cu}}$ luminesced much less intensely (fig. S9, red) as a consequence of possible fluorescence quenching by Cu^{2+} in the coordination network around the nanotube. These contrasting luminescence features allowed us to investigate whether the two graphite-like nanotubular segments in *block*-$\mathbf{NT_{1\cdot Cu}/NT_2}$ (Fig. 1C) communicate with one another by excitation energy transfer over the heterojunction interface. When an acetone dispersion of *block*-$\mathbf{NT_{1\cdot Cu}/NT_2}$ prepared by using the mole ratio [**2**]/[**1**] of 0.5 for the stepwise coassembly was photoexcited at 365 nm, the observed fluorescence (Fig. 3B, pink) was as weak as that of homotropically assembled $\mathbf{NT_{1\cdot Cu}}$ (Fig. 3B, red). Even when the mole ratio [**2**]/[**1**] used for the stepwise coassembly was increased from 0.5 to 1.0 (orange), 1.5 (green), and 2.0 (blue) (Fig. 3A), the fluorescence intensity of *block*-$\mathbf{NT_{1\cdot Cu}/NT_2}$ remained almost unchanged at a very low level (Fig. 3B). In contrast to *block*-$\mathbf{NT_{1\cdot Cu}/NT_2}$ (Fig. 3B inset), a mixture of homotropic $\mathbf{NT_{1\cdot Cu}}$ and $\mathbf{NT_2}$ ([**2**]/[**1**] = 1.0) (Fig. 3C, orange) displayed a rather bright fluorescence (Fig. 3D inset), where the observed intensity was the sum of those of $\mathbf{NT_{1\cdot Cu}}$ and $\mathbf{NT_2}$ (Fig. 3D, orange). When the mixing ratio of $\mathbf{NT_2}$ to $\mathbf{NT_{1\cdot Cu}}$ was varied ([**2**]/[**1**] = 0.5 to 2.0) (Fig. 3C), the overall fluorescence intensity changed depending on the amount of $\mathbf{NT_2}$ (Fig. 3D). Together with the results of these control experiments, the fluorescing properties observed for *block*-$\mathbf{NT_{1\cdot Cu}/NT_2}$ indicate that the $\mathbf{NT_{1\cdot Cu}}$ and $\mathbf{NT_2}$ segments communicate efficiently over the heterojunction interface (Fig. 1D) by excitation energy transfer. The results also suggest that the amount of unconnected $\mathbf{NT_2}$, if any formed in the stepwise coassembly (Fig. 1C), is negligibly small.

Because the excitation energy transfers over the heterojunction interface from one nanotubular segment ($\mathbf{NT_2}$) to the other ($\mathbf{NT_{1\cdot Cu}}$) in *block*-$\mathbf{NT_{1\cdot Cu}/NT_2}$ (Fig. 1C), we were motivated to explore the behaviors of charge carriers, if generated, in *block*-$\mathbf{NT_{1\cdot Cu}/NT_2}$. For this purpose, we used a flash-photolysis time-resolved microwave conductivity (FP-TRMC) method (*30*), which allows for evaluating the intrinsic properties of charge carriers without electrodes. At first, we investigated the FP-TRMC profiles of homotropically assembled $\mathbf{NT_{1\cdot Cu}}$ and $\mathbf{NT_2}$. Upon laser excitation at 355 nm (photon density, 4.7×10^{15} cm^{-2}), both nanotube samples in the solid state displayed TRMC signals, indicating that these nanotubes are photoconductive. The TRMC signals thus observed for $\mathbf{NT_{1\cdot Cu}}$ and $\mathbf{NT_2}$ decayed at comparable rates (fig. S10, A and B) with lifetimes ($\tau_{1/e}$) of 1.4×10^{-6} and 2.5×10^{-6} s, respectively (Fig. 4). Of particular interest to note here, the charge carriers generated in *block*-$\mathbf{NT_{1\cdot Cu}/NT_2}$ ([**2**]/[**1**] = 1.0) were long-lived (fig. S10D): The observed lifetime ($\tau_{1/e}$ = 8.8×10^{-6} s) was roughly five times longer than those of $\mathbf{NT_{1\cdot Cu}}$ and $\mathbf{NT_2}$ (Fig. 4). Taking into account the energy levels of **1** (*16*) and **2** (fig. S11) estimated from their electrochemical and spectral data, it is most likely that the $\mathbf{NT_{1\cdot Cu}}$ and $\mathbf{NT_2}$ segments preferentially accommodate hole and electron, respectively. As a consequence of such preferential localization of hole and electron in *block*-$\mathbf{NT_{1\cdot Cu}/NT_2}$, the probability of charge recombination could be reduced. In sharp contrast, a mixture of homotropic $\mathbf{NT_{1\cdot Cu}}$ and $\mathbf{NT_2}$ ([**2**]/[**1**] = 1.0) (fig. S10C) hardly showed suppression of charge recombination ($\tau_{1/e} = 2.0 \times 10^{-6}$ s) (Fig. 4).

The behaviors of excitons and charge carriers thus observed for semiconducting *block*-$\mathbf{NT_{1\cdot Cu}/NT_2}$ are remarkable considering that they are brought about only by noncovalent connection of two different homotropic blocks with

Downloaded from www.sciencemag.org on November 14, 2011

an extremely thin (~3 nm) facet. In particular, the nearly perfect fluorescence quenching of its NT_2 block substantiates that electronic effects of heterojunctions can indeed propagate over a micrometer-long distance through a great number of π-stacks in semiconducting organic materials.

References and Notes

1. M. T. Björk *et al.*, *Nano Lett.* **2**, 87 (2002).
2. S. Banerjee, S. S. Wong, *Nano Lett.* **2**, 195 (2002).
3. O. Harnack, C. Pacholski, H. Weller, A. Yasuda, J. M. Wessels, *Nano Lett.* **3**, 1097 (2003).
4. B. Tian *et al.*, *Nature* **449**, 885 (2007).
5. A. I. Hochbaum, P. Yang, *Chem. Rev.* **110**, 527 (2010).
6. F.-S. Tsai *et al.*, *Appl. Phys. Express* **4**, 025002 (2011).
7. S. Günes, H. Neugebauer, N. S. Sariciftci, *Chem. Rev.* **107**, 1324 (2007).
8. B. C. Thompson, J. M. J. Fréchet, *Angew. Chem. Int. Ed.* **47**, 58 (2008).
9. G. Yu, J. Gao, J. C. Hummelen, F. Wudl, A. J. Heeger, *Science* **270**, 1789 (1995).
10. P. Peumans, S. Uchida, S. R. Forrest, *Nature* **425**, 158 (2003).
11. G. Li *et al.*, *Nat. Mater.* **4**, 864 (2005).
12. J. Y. Kim *et al.*, *Science* **317**, 222 (2007).
13. T. F. A. De Greef *et al.*, *Chem. Rev.* **109**, 5687 (2009).
14. F. J. M. Hoeben, P. Jonkheijm, E. W. Meijer, A. P. H. J. Schenning, *Chem. Rev.* **105**, 1491 (2005).
15. F. Würthner *et al.*, *J. Am. Chem. Soc.* **126**, 10611 (2004).
16. Y. Yamamoto *et al.*, *Science* **314**, 1761 (2006).
17. A. L. Sisson *et al.*, *Angew. Chem. Int. Ed.* **47**, 3727 (2008).
18. Y. Yamamoto *et al.*, *Proc. Natl. Acad. Sci. U.S.A.* **106**, 21051 (2009).
19. N. Sakai, R. Bhosale, D. Emery, J. Mareda, S. Matile, *J. Am. Chem. Soc.* **132**, 6923 (2010).
20. By using crystallizable core units, the formation of rodlike block co-micelles has been demonstrated (*21–24*).
21. X. Wang *et al.*, *Science* **317**, 644 (2007).
22. T. Gädt, N. S. Ieong, G. Cambridge, M. A. Winnik, I. Manners, *Nat. Mater.* **8**, 144 (2009).
23. J. B. Gilroy *et al.*, *Nat. Chem.* **2**, 566 (2010).
24. S. K. Patra *et al.*, *J. Am. Chem. Soc.* **133**, 8842 (2011).
25. J. P. Hill *et al.*, *Science* **304**, 1481 (2004).
26. W. Jin *et al.*, *J. Am. Chem. Soc.* **130**, 9434 (2008).
27. Materials and methods are available as supporting material on *Science* Online.
28. W. Zhang, W. Jin, T. Fukushima, N. Ishii, T. Aida, *Angew. Chem. Int. Ed.* **48**, 4747 (2009).
29. G. Zhang *et al.*, *J. Am. Chem. Soc.* **129**, 719 (2007).
30. A. Saeki, T. Fukumatsu, S. Seki, *Macromolecules* **44**, 3416 (2011).

Acknowledgments: We thank E. Ohta (RIKEN) for DFT calculation of HBC **2**. W.Z. thanks the Japan Society for the Promotion of Science Young Scientist Fellowship (21•9925). T.F. thanks Ministry of Education, Culture, Sports, Science, and Technology, Japan, for financial support (21350108).

Supporting Online Material

www.sciencemag.org/cgi/content/full/334/6054/340/DC1
Materials and Methods
Figs. S1 to S11
References (*31–33*)

27 June 2011; accepted 14 September 2011
10.1126/science.1210369

Dynamics of the Reaction of Methane with Chlorine Atom on an Accurate Potential Energy Surface

Gábor Czakó* and Joel M. Bowman

The reaction of the chlorine atom with methane has been the focus of numerous studies that aim to test, extend, and/or modify our understanding of mode-selective reactivity in polyatomic systems. To this point, theory has largely been unable to provide accurate results in comparison with experiments. Here, we report an accurate global potential energy surface for this reaction. Quasi-classical trajectory calculations using this surface achieve excellent agreement with experiment on the rotational distributions of the hydrogen chloride (HCl) product. For the $Cl + CHD_3 \rightarrow HCl + CD_3$ reaction at low collision energies, we confirm the unexpected experimental finding that CH-stretch excitation is no more effective in activating this late-barrier reaction than is the translational energy, which is in contradiction to expectations based on results for many atom-diatom reactions.

Decades of experimental and theoretical studies of atom-diatom reactions led to a well-validated framework for predicting the effect of vibrational excitation on the ensuing dynamics (*1*, *2*). Earlier fundamental research demonstrated the importance of the reaction barrier location on the efficacy of partitioning the total energy between internal excitation of the diatomic molecule and relative translational energy of the reactants. The careful and correct analysis of these reactions led to the "Polanyi rules" (*3*), which state that vibrational energy is more efficient than is translational energy in activating a late-barrier reaction, whereas the reverse is true for an early-barrier reaction. Recent studies have investigated the generality and validity of these paradigms for polyatomic systems. The X + methane (CH_4 and deuterated isotopologues) reactions (which replace the diatomic with a five-atom molecule) have played a central role in this research, in which, for example, the choice of X as H, O, F, and Cl has permitted the height and location of the reaction barrier to vary widely. Recent experiments by Liu and co-workers (*4–8*) on the F and Cl + methane reactions have uncovered surprising departures from expectations that present a strong challenge to theory, which ultimately provides detailed understanding of chemical reaction dynamics. A rigorous theoretical approach to reaction analysis consists of two components. The first is to determine the global potential energy surface (PES) (*9*), which governs the nuclear motion, and the second is to perform dynamics calculations with the PES. We succeeded in carrying out this process recently for the early-low-barrier $F + CHD_3$ reaction, for which we were able to illuminate the surprising experimental result of the enhancement of the $DF + CHD_2$ channel by exciting the CH-stretch (*10*, *11*). In this Report, we take the same approach to address and interpret experiments on the late-high-barrier $Cl + CHD_3$ reaction by Liu and co-workers (*5*), which also uncovered a surprising result, namely that at low collision energies (E_{coll}) vibrational excitation of the CH-stretch was no more effective than was translational energy in promoting the reaction. This result, as pointed out by these authors, contradicts the rule of thumb of reaction dynamics (Polanyi rules). Other interesting experimental results of this reaction are also successfully addressed.

As with the previous accurate PES for $F + CH_4$ (*10*), the $Cl + CH_4$ PES is a permutationally invariant fit (*12*, *9*) to roughly 16,000 high-level ab initio electronic energies. The selection of configurations for the PES is quite similar to procedures used for the $F + CH_4$ PES (*10*, *12*), and details are given in (*13*). A key part of this approach is the use of an electronic structure method that gives accurate energies, especially for the barrier height, reaction enthalpy, and the entrance and exit channel van der Waals (vdW) wells. These wells, which result from long-range attractive interactions, are ubiquitous in chemistry, and as we show here, the prereactive one has a substantial effect on the $Cl + CHD_3$ reaction dynamics at low collision energies. The inclusion of the spin-orbit (SO) correction is also essential in the present case because it effectively increases the barrier height and reaction endoergicity by 0.8 kcal/mol and has a substantial effect on the entrance channel vdW well. (The SO correction is a relativistic effect, which lowers the energy of the halogen atoms and has about twice as large an energy shift on the heavier Cl than on F. The widely applied nonrelativistic electronic structure computations neglect this effect.) There is also a substantial basis set–superposition error in this region, which has to be corrected. Thus, the goal for the present PES is to take all of this into account. In order to achieve this goal, we used a composite electronic structure method, which provides accurate energies with affordable computational time. The general composite approach (*14*), which is widely used, combines results from several levels of ab initio method and basis (*15*, *16*). Second, in order to account for the SO effect differences between the SO and non-SO ground-state electronic energies, obtained by means of multireference configuration interaction (MRCI) with Davidson correction (MRCI + Q) with basis set aug-cc-pVTZ (MRCI + Q/aug-cc-pVTZ), were added to

Cherry L. Emerson Center for Scientific Computation and Department of Chemistry, Emory University, Atlanta, GA 30322, USA.

*To whom correspondence should be addressed. E-mail: czako@chem.elte.hu

Downloaded from www.sciencemag.org on November 14, 2011